Sucker Rod Pump Working State Diagnosis Using Motor Data and Hidden Conditional Random Fields

Boyuan Zheng, *Student Member, IEEE,* Xianwen Gao, and Rong Pan, *Senior Member, IEEE*

***Abstract*—In oil exploitation, the short maintenance period and poor real-time performance of dynamometer card sensors limit the timely working state diagnosis for sucker rod pumps (SRP). The motor is the power source of the SRP that provides all the energy required to lift the oil from underground to surface. The motor power output is highly associated with the working state of the entire equipment. Thus, this paper proposes a new strategy to predict the working state of SRP based on motor power. First, seven novel features are extracted from motor power data to support the modeling and diagnosing processes, with the consideration of the significant parameters such as valve's working points and the operating cycle of SRP. Moreover, a custom-designed multiple hidden conditional random fields model with time window is employed as the classifier to identify different working states. At last, the proposed method is validated by a set of motor power data collected from wells by a self-developed device. The experimental result demonstrates the effectiveness of the proposed method for the working state diagnosis of SRPs.**

***Index Terms*— Diagnosis, Motor Power Data, Sucker Rod Pump, Hidden Conditional Random Fields**

I. Introduction

Sucker rod pumps are the widely used lifting equipment for recovering oil in oil fields. In practice, the sucker rod has an up-and-down movement driven by a motor through mechanical parts and pulls oil liquid to the ground. The structure diagram of a typical sucker rod pump is shown in Fig. 1. Because the working environment of down-hole is very harsh, many faulty working states frequently occur. Currently, offline manual inspection is still the most common approach to monitor the working state in oilfields, but it is clear that this approach suffers from the unavailability of real-time working state and the subjectivity of engineer's judgment.

As a result, many computer-aided diagnosis methods have been proposed to deal with this problem [1, 2]. Some earlier works, for example, Derek et al. [3], built the experience-based expert system to assist engineers in monitoring and diagnosing the subsurface problem of SRP. However, this method is in general difficult to be implemented as it overly relays on the subjective judgment of the rule-maker. As an alternative, the dynamometer card (DC) -based intelligent diagnosis method has been proposed [4], [5]. Xu et al. [6] presented a self-organizing neural network model for monitoring the working state of SRP and used the collected DC data to test the proposed model. In [7], Li et al. used two different DC-based methods to address the SRP diagnosis problem. The first method utilized a piecewise analysis method for analyzing DC data and a novel Extreme Learning Machine was employed as the diagnosis model. Zhang et al. [8] mapped the data between different wells into the same subspace, to eliminate the distribution difference between the data and solve the problem of incomplete data, and established the rod pump operating condition diagnosis model under the framework of the supervised dictionary. Zheng and Gao [9] analyzed the vital characteristics of the SRP working process and proposed a new piecewise strategy to extract features from DCs, and used these features to build a Hidden Markov Model (HMM) for SRP working state diagnosis.

Distinctly, the above computer-aided method are all based on DCs that are collected by a sensor installed on the polished rod

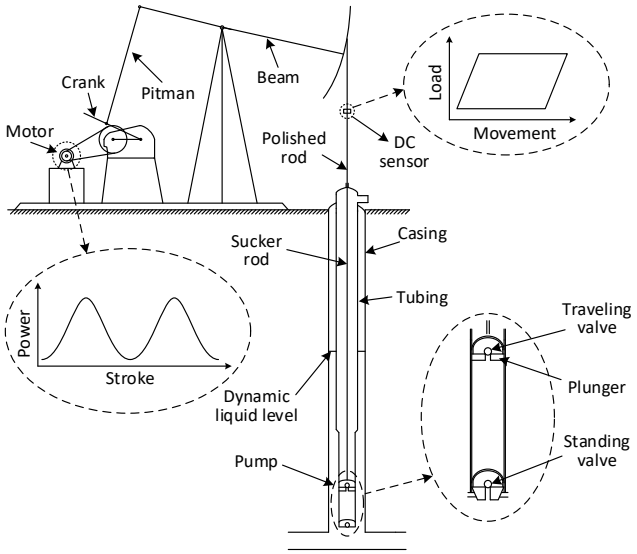

Fig. 1. Sucker rod pump system

Manuscript received March 1, 2019; revised June 27, 2019; accepted September 11, 2019. This work was supported in part by the National Natural Science Foundation of China under grant 61573088 and 61573087, in part by the China Scholarship Council under grant [2018] 3101. *(Corresponding author: Xianwen Gao)*

B. Zheng and X. Gao are with the Department of Information Science and Engineering, Northeastern University, Shenyang, China (e-mail: zhengboyuanneu@163.com; gaoxianwen@mail.neu.edu.cn).

R. Pan is with the School of Computing, Informatics, and Decision Systems Engineering, Arizona State University, Tempe, USA (e-mail: rong.pan@asu.edu)

as shown in the Fig.1. However, in practice, this type of sensor is very expensive and the safety issue of installing it on the rod is of concern too. Hence, this paper aims to address the SRP diagnosis problem from a new angle that takes motor power as an alternative data source. To identify different working states based on this new type of data, two analytic steps are required – feature extraction and statistical modeling of faulty states.

As a time-series signal, currently, the motor power signals are most common being analyzed by frequency domain-based and time domain-based methods in applications [10], [11], such as FFT and Wavelet. However, these kind of methods may not adequately consider the mechanism of SRP and thus unsuitable for motor power feature extraction. Therefore, developing an approach to extract meaningful features from motor power data is the first step to be carried out.

The next step, statistical modeling, is the foundation of faulty diagnosis. In a previous work [8], the authors had implemented a method based on HMM, offering satisfactory results. In recent years, the Conditional Random Fields [12-15], as a discriminative model, has been widely used in many research areas due to its outstanding theoretical basis and model structure [16-18]. As an improved design for classification problems, the Hidden Conditional Random Fields (HCRFs) [19], [20] has several advantages than HMM. The HCRFs retains the properties of state transition description and avoids the complicated computation on prior distribution of observations. These advantages had been thoroughly discussed in previous literature [21], [22]. Furthermore, considering the application of this paper, HCRFs has an advanced form to address the recognition of time-series signals, as it considers not only the current observation vector but also the adjacent vectors, which means that the HCRFs is able to better handle any possible changing tendency within time series.

Inspired by the above studies, we propose a new methodology for SRP diagnosis in this paper. Our contributions are given as follows: Firstly, based on the mechanism analysis of the working cycle of pumps, we devise a novel segmentation strategy to be applied on motor power curves and extract seven meaningful features that are related to the positions and states of valves. Secondly, a multiple working state diagnostic method is developed, which is able to distinguish different types of faulty states. Furthermore, in order to construct the diagnosis model more effectively, a new feature function is designed that is based on the consideration of SRP mechanism and data distribution. Finally, a self-developed device is used to collect data from the oil field and the experimental results demonstrate the superiority of the proposed method.

II. Feature Extraction from The Motor Power Data

A. Operating mechanism analysis of the SRP

The working cycle of motor power along with the polished rod movement and pump operation is shown in Fig 2. At the theoretically normal working state, the motor power curve consists of two peaks that are equal. Driven by the motor, the plunger moves up-and-down and the valves of pump become open and closed in cycle. To understand this process we may place Fig. 1 and Fig. 2 side-by-side. With the movement of the plunger, the pressure in the pump chamber changes. In the first half stroke, called up-stroke, the pressure in pump chamber decreases as the plunger moves up, so the standing valve opens (see the second illustration in the bottom panel of Fig. 2) and oils flow into the pump chamber. In the second half stroke, called up-stroke, the plunger travels down and discharges the oil in the pump chamber through the standing valve into tubing (see the forth illustration in the bottom panel of Fig. 2).

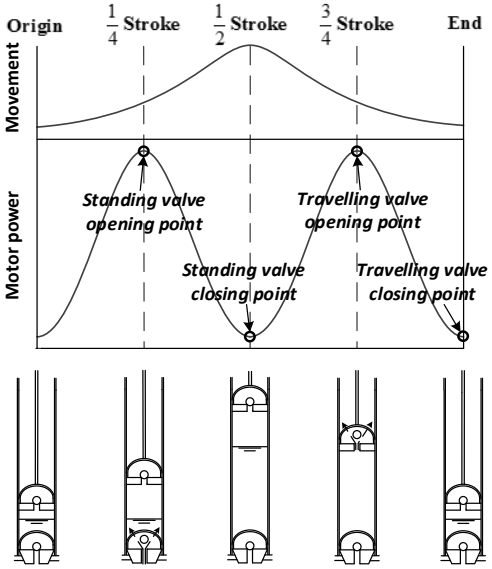

Fig. 2. Working process of motor power in one stroke.

Notably, as shown in the middle panel of Fig. 2, four points are marked on the peaks and valleys of motor power curve to denote the working points of valves. These marked points reflect the working states of the pump, as their positions are going to change if the pump is at a faulty state. Hence, this section proposes a method to obtain seven features based on the calculation of these valves' working points.

B. The valve's working positions on the motor power curve

Considering the valve's working points on the motor power curve, we can utilize maximum variation of curvature to figure out these points. For a parametric curve, curvature is defined by

$$C(i)=\frac{x_i'y_i''-x_i''y_i'}{\left[x_i'^2+y_i'^2\right]^{3/2}} \tag{1}$$

As the data of motor power output consist of measurements at discrete time points, thus, the Eq. (2) is employed to calculate the curvature at each time point on the motor power curve, and then Eq. (3) is used to determine the change in curvature.

$$C(i)=\frac{\left[\bar{x}_i-\bar{x}_{i-1}\right]\left[\bar{y}_i-2\bar{y}_{i-1}+\bar{y}_{i-2}\right]-\left[\bar{x}_i-2\bar{x}_{i-1}+\bar{x}_{i-2}\right]\left[\bar{y}_i-\bar{y}_{i-1}\right]}{\left[\bar{x}_i{}^2+\bar{y}_i{}^2-2\bar{x}_i\bar{x}_{i-1}-2\bar{y}_i\bar{y}_{i-1}+\bar{x}_{i-1}{}^2+\bar{y}_{i-1}{}^2\right]^{3/2}} \tag{2}$$

$$\Delta C=\left|C(i)-C(i-1)\right| \tag{3}$$

Now, the maximum changing point of curvature can be found by

$$\max\left[\Delta C(i)\right] \quad i=1,2,\ldots,n \tag{4}$$

Eqs. 2-4 are devised to find the valves' working positions based on locating the position where the max change of curvature occurs. However, in practice, the shapes of motor curves are irregular at most of the time caused by faulty states and noise. It may be difficult to obtain accurate valve working points by only considering the change of curvature. Hence, a new method is presented to cope with this problem.

C. Average Power Segmentation

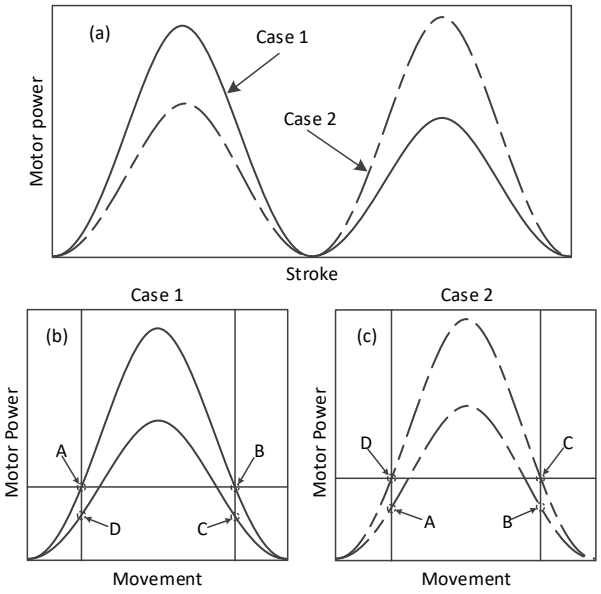

Fig. 3. Average power segmentation method for different abnormal cases

Fig. 3(a) presents the two forms of faulty motor power curves that have different shapes. Case 1 has a higher crest during up-strokes and a lower crest during down-strokes, while Case 2 has the opposite pattern.

In order to locate the exact positions of the valve working points on the motor power curves, Figs. 3(b) and 3(c) illustrate a novel method, called Average Power Segmentation, to obtain the potential regions for locating valve working points on the curves at different working states. Unlike Fig. 3(a), Figs. 3(b) and 3(c) are drawn with the abscissa as the polished rod's movement, which is designed to offer a clear way to carry out the following analysis.

As shown in Figs. 3(b) and 3(c), both motor power curves are segmented by three lines – one horizontal line and two vertical lines. The horizon line is drawn at the average motor power and the two vertical lines are drawn from the abscissa of the intersections of average power and motor power curve. For example, in case 1, when the up-stroke has higher power, the intersections of the horizon line and motor power curve are A and B, then two vertical lines can be found based on the horizon positions of A and B. As a result, the additional points, C and D, are determined. Finally, the motor power curve is partitioned into four regions (D-A, A-B, B-C, and C-D), which are the potential regions for locating the four valve working points. In the case 2, when the down-stroke has higher power, the A and B are figure out based on the positions of C and D that are determined by average motor power.

D. Seven features of motor power data

After identifying the four working points, we propose to use the following seven variables as the features of a motor power curve.

The first three features, L_a, L_b, and L_c, use three different distances to characterize the motor power curve. The first one is the distance L_a between the standing valve opening position and the standing valve opening position:

$$L_a=\sqrt{\left[S_{vo}(x)-T_{vo}(x)\right]^2-\left[S_{vo}(y)-T_{vo}(y)\right]^2} \tag{5}$$

where, $S_{vo}(x)$ and $S_{vo}(y)$ are the abscissa and the ordinate of the standing valve opening position, respectively, $T_{vo}(x)$ and $T_{vo}(y)$ are the abscissae and the ordinate of the standing valve opening position, respectively.

The second one is the distance L_b between the standing valve opening position and the standing valve closing position:

$$L_b=\sqrt{\left[S_{vo}(x)-S_{vc}(x)\right]^2-\left[S_{vo}(y)-S_{vc}(y)\right]^2} \tag{6}$$

where, $S_{vc}(x)$ and $S_{vc}(y)$ are the abscissa and ordinate of the standing valve closing position, respectively.

The third one is the distance L_c between the standing valve opening position and the standing valve closing position:

$$L_c=\sqrt{\left[T_{vo}(x)-T_{vc}(x)\right]^2-\left[T_{vo}(y)-T_{vc}(y)\right]^2} \tag{7}$$

where, $T_{vc}(x)$ and $T_{vc}(y)$ are the abscissae and the ordinate of the standing valve closing position, respectively.

The fourth feature describes the work of up-stroke, W_{up},

$$w_{up}=\frac{1}{w}\int_{t_0}^{t_1} motor\ power \tag{8}$$

$$w=\int motor\ power \tag{9}$$

where w is the work in one stroke, t_0 is the beginning of upstroke, and t_1 is the end of upstroke.

The fifth feature describes the work of down-stroke, W_{down},

$$w_{down}=\frac{1}{w}\int_{t_1}^{t_2} motor\ power \tag{10}$$

where t_2 is the end of downstroke.

At faulty working states, the negative power often occurs due to the infliction to motor caused by the change of load. Hence, the sixth feature is the ratio between negative work and positive work:

$$R_{NP}=\int_0^{t_n} motor\ power \Big/ \int_0^{t_p} motor\ power \tag{11}$$

where t_n is the cumulative time of negative power and t_p is the cumulative time of positive power.

As another important feature, the ratio between average motor power and rated power can reflect the entire work in one stroke; therefore, it is employed as the seventh feature:

$$R_{pr} = \frac{\sum_{i=1}^{N_s} P_i}{N_s \times P_{rated}} \tag{12}$$

where N_s is the number of samples in one stroke, and P_{rated} stands for the rated power of the motor.

III. SRP Working State Diagnosis Using MHCRFs

A. MHCRFs for diagnosis

We presents an observation sequence $O = \{O_1, O_2, \ldots, O_T\}$. Each observation O_t is represents a feature vector that belongs to space $\Re^d$, where d is the number of features. HCRFs model is designed to identify the mapping between O and class label $y_i \in \{y_1, y_2, \ldots, y_N\}$ that stands for the working states to be considered in this paper. In this mapping, a sequence made of hidden variables $H = \{h_1, h_2, \ldots, h_T\}$ that are not directly observable is used to encode the joint distribution between label y and given observations O [22]. The HCRF models the conditional probability of a label given O by:

$$P(y \mid O;\Theta) = \frac{\sum_{h \in H} \exp\{\phi(y,h,O;\Theta)\}}{\sum_{y' \in Y}\sum_{h \in H} \exp\{\phi(y',h,O;\Theta)\}} \tag{13}$$

where Θ is the parameter set of the model, y' is one possible labels, and ϕ is the feature function.

In this paper, we consider that an SRP may be operated in various working states. Beside of *Normal*, we are interested in five faulty states that are listed as follows:

Gas affected: At the beginning of up-stroke, there exists abundant remaining gas in the pump and it affects the operation of the pump.

Insufficient liquid supply: During the oil production process, the liquid supply often goes down after a long operation period which is caused by the decreasing oil reservoir pressure, and which in turn would result in low yield.

Gas locked: When the amount of the gas in the pump is abundant enough to stop valves from working, the valves can barely be open at any time during a stroke, which leads to extremely low yield.

Standing valve leakage: After a long time of operation in the harsh environment, the standing valve may undergo some damages due to wear-out, which may cause liquids leaking through the broken parts.

Parting rod: After a long operating period in down-hole, due to mechanical wear, fatigue damage and corrosion damage will appear on sucker rod.

After receiving the motor power data at the six working states specified above, the observed sequences of features are obtained based on the algorithm in Section II. The purpose of MHCRFs model is to build the distribution models for all working states based on these observations and to identify the states based on their distributions. Fig. 4 provides a simplified schematic plot (in a two-dimensional space) of this model. The clusters in this figure denote the data of six working states projected on a two-dimension space.

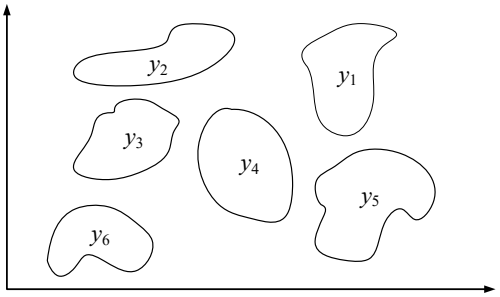

Fig. 4. The projection of data in the two-dimensional space

Fig 4 illustrates six groups of data sampled from six working states. Hence, in this paper, the observation sequence can be defined as follows:

$$O^{(N)} = \{O_1, O_2, \ldots, O_6\} \tag{14}$$

$$O_i = \{O_i^1, O_i^2, \ldots, O_i^T\} \tag{15}$$

where O_i is the observation sequence of ith working state and O_i^j is a feature vector extracted from the jth motor power curve at the ith working state through the proposed method in Section II.

According to the structure of the observation sequence, in this paper we construct a Multiple HCRFs (MHCRFs), which is defined as follows:

$$\Theta^{(N)} = \{\Theta_1, \Theta_2, \ldots, \Theta_6\} \tag{16}$$

where $\Theta^{(N)}$ is the model parameter set and Θ_i is the model parameters corresponding to the ith working state.

Based on this modeling framework, for the ith model with parameter Θ_i, we maximize the following log-likelihood function to find the unknown parameters:

$$L(\Theta_i) = \sum_{i=1}^{n} \log P(y_i \mid O_i, \Theta_i) - \frac{\|\Theta_i\|^2}{2\sigma^2} \tag{17}$$

where 'log' denotes the natural logarithm function and y_i is the label of the ith working condition. The second term of the right hand side of Eq. (17) is a Gaussian prior with variance σ^2 to regularize the training. In this study, we used the gradient ascent of the conditional maximum likelihood to search the optimal parameters of the ith model:

$$\Theta_i^* = \arg\max L(\Theta_i) \tag{18}$$

During the searching process, the feature functions, which is the function $\phi(\cdot)$ defined in Eq. (13), is applied for fitting observed data. Within this function, two sub-functions, $T(\cdot)$ and $E(\cdot)$, are designed to represent the transmission behaviors among different states and the relationship between state and observed feature sequence. However, this original design of the function may not be appropriate for a diagnosis problem. Firstly, according to the proposed framework, for a single

model Θ_i, the samples of the training set is taken at the same working state, which means the state transmission would not happen in the training data. Secondly, considering the operation circumstance of SRP, its state may gradually change over time due to the change in liquid flow and underground pressure. If this slow change process is ignored, the performance of our model will be detrimentally affected.

Therefore, inspired by [23], we design a new feature function by adding a time window to compensate the working-point drift of SRP. The new feature function is defined as follows:

$$\begin{aligned}\phi(h_i, O_i; \Theta_i, W) = \alpha \sum_{w=T-W}^{T} \mu_w E\left(h_t, O_i^w; \Theta_i\right) \\ + (1-\alpha) \sum_{m=1}^{M} \mu_m E\left(h_t, O_i; \Theta_i\right)\end{aligned} \tag{19}$$

where α is a weight parameter of the window and $0 \le \alpha \le 1$, T is the number of samples of the i^{th} working state, W is the window size, and M is the total number of feature functions that relates observations to the current operating mode. The parameter μ_w and μ_m represent the weight factors for feature functions that play the same role as an emission probability matrix under the HMM scheme. The function $E(\cdot)$ is defined as follows:

$$E\left(h_i, O_i, \Theta_i\right) = E\left(h_i, O_i^1, O_i^2, \ldots, O_i^T\right) = \begin{bmatrix} E_1\left(h_i, O_i^1\right) \\ E_2\left(h_i, O_i^2\right) \\ \vdots \\ E_T\left(h_i, O_i^T\right) \end{bmatrix} \tag{20}$$

The elements in the vector are all assumed to be indicator functions as

$$E_l\left(h_i, O^t\right) = \begin{cases} 1 & if\ O^t \in B \\ 0 & otherwise \end{cases} \tag{21}$$

where $l = 1, 2, \ldots, T$, and B stands for the finite observation set.

In order to obtain the parameter set $\Theta^{(N)}$ as shown in Eq. (16), the proposed method should be supplied with the data from all six working modes to complete the training procedure.

For a testing data set at time $T+1$, its working state can be predicted by comparing the likelihoods calculated by the model with $\Theta^{(N)}$, while the highest log-likelihood corresponds to the prediction result; i.e.,

$$\arg\max P\left(y \mid O^{T+1}, \Theta^{(N)}\right) \tag{22}$$

where $\Theta^{(N)}$ is the trained model parameter set and all sub-models are obtained from the training process.

B. The framework of the proposed method

Fig. 5 illustrated the framework of the proposed method, which consists of two parts. The first part is the Model Training part, as drawn on the top half of this figure, which is designed to establish the diagnosis model. The detailed steps are as follows:

Step 1: Collect the historical motor power samples from wells under different working states.

Step 2: Conduct the feature extraction on the historical samples.

Step 3: Train the models set $\Theta^{(N)}$ using the features vectors in $O^{(N)}$.

The second part is the Diagnosing part, as drawn on the bottom half of this figure. This part aims to identify and decide on the current working state of a well using real-time data. Its implementation steps are as follows:

Step 1: Collect the real-time motor power sample from wells.

Step 2: Extract the feature vector of this real-time sample.

Step 3: Diagnose the working state of the well based on the trained diagnosis models and Eq. (22).

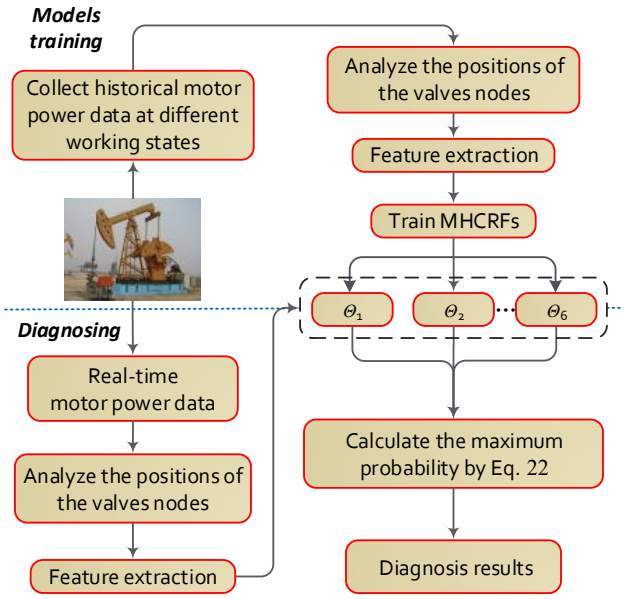

Fig. 5. Flowchart of the SRP diagnosis by the proposed method

IV. Experimental Results

A. Data collection

The motor power data are collected by a device, called NEU Monitor, which was developed by the research team in Northeastern University, China. As shown in Fig. 6(a), the three-phase asynchronous motor is typical electrical driving equipment for the SRP. In order to give the working currents and voltages to the NEU Monitor, six transducers are installed on the power entrance of the motor. The core chip in this monitor for collecting motor power is ATT7022B that is able to measure active motor power by calculating the power factor continually. This ability is important for measuring the exact motor power of SRP and giving a reliable support for the following data analysis, as motor efficiency undergoes considerable variations with the changes of the applied load torque in operation. The proximity switch is another important component that is used to measure the working period of the SRP by detecting the moving trajectory of the crank. Beside of data collection, this device can also perform several data analysis functions (i.e., diagnosis for working state and soft-sensor for dynamic liquid level), as well as data storage, data query, and data display. As shown in Fig. 6 (b), a picture of field installation, in order to avoid damages from the harsh operating environment, the chips and circuits are placed in a

cabinet. In addition, a Liquid Crystal Display and the Membrane Switches are installed on the surface of this cabinet to facilitate data display and data query.

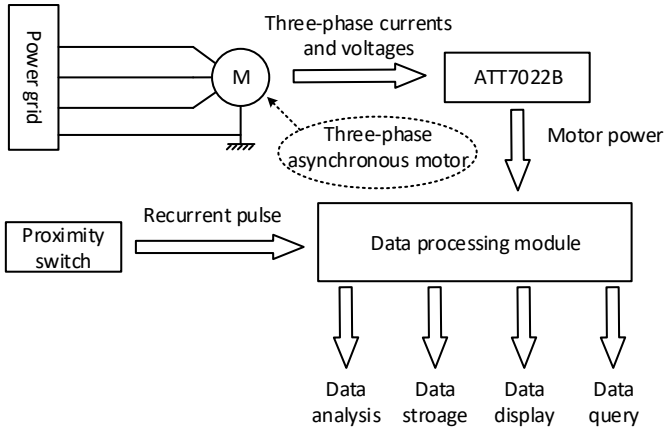

(a) Schematic diagram of monitoring instrument

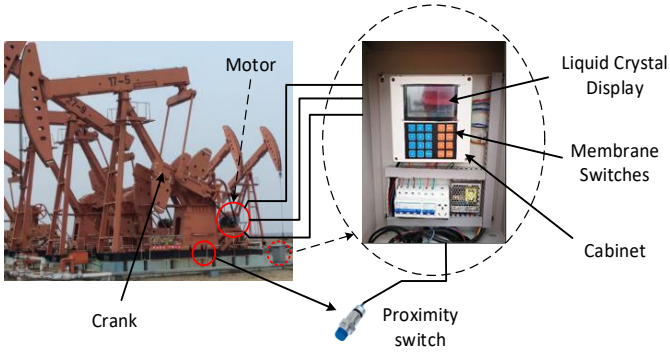

(b) Installation of the monitoring instrument

Fig. 6. The application of monitoring system for the SRP

After long-term practice in oil field, a set of motor power data under six working states were collected from six wells using NEU monitor. This set of data are used to verify the proposed method in the paper. For convenience, the six wells are named as #1 to #6 corresponding to six working states, namely *Normal*, *Insufficient Liquid Supply*, *Gas affected*, *Gas locked*, *Standing valve leakage*, and *Parting rod*.

In this data set, there are 1200 labeled samples that are collected under six working states. Each sample is the motor power data in one stroke. As for each working state, 200 samples are collected in an equal time interval. The first 160 samples are utilized as the training set for building the diagnosis model and the reminding samples are used as the testing set. Before modeling and diagnosis, the proposed method in Eqs. (5) to (12) is employed to extract features vectors from the samples.

B. Feature analysis of motor power data

1) Valve working points on the motor power curve

After obtaining the oil field data, a pretreatment of data to reduce the interference from noise is necessary. In this study, a moving average filter is adopted to remove the noise in the motor power data, which is

$$K(t)=\frac{1}{5}\sum_{t-2}^{t+2}k(t) \tag{23}$$

where the $K(t)$ is the filtered motor power data at time t.

In order to verify the proposed segmentation algorithm for identifying the valve's working points, the following example of a real motor power curve is run.

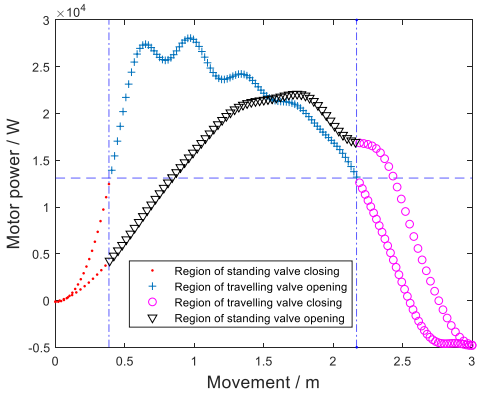

Fig. 7. Average motor power segmentation on a collected sample

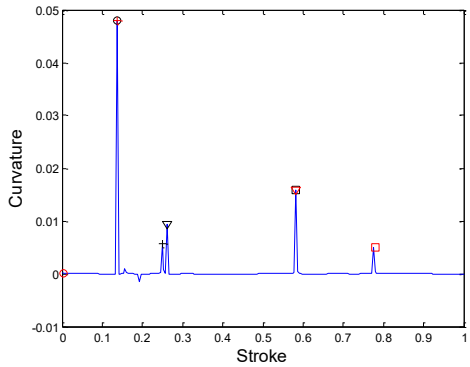

Fig. 8. Valve working points on curvature based on different strategies

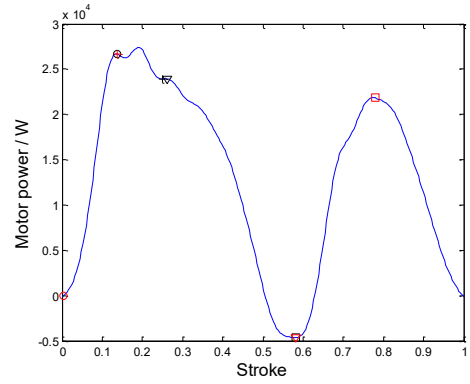

Fig. 9. Valve working points on motor power curve based on different strategies

The first step of feature extraction is to segment the motor power curve into four parts to give the potential areas for finding the valve's working points. According to the proposed strategy in Section II, the average power is applied to the segmentation as shown in Fig. 7. In this figure, the horizontal line is the average motor power and the two vertical lines are the abscissa of the intersections of average power and motor power curve. To help the illustration, the samples are depicted

TABLE I
AVERAGE DIGITIZED RESULTS OF FEATURE DISTRIBUTION OF ALL THE COLLECTED DATA

Working state	*Proposed features*						
	L_a	L_b	L_c	w_{up}	w_{down}	R_{NP}	R_{pr}
Normal	0.9144	1.0427	0.9762	0.5130	0.4870	0.0107	0.3626
Insufficient Liquid Supply	0.5982	0.9302	1.0543	0.2980	0.7020	0.1036	0.1271
Gas affected	0.8373	1.0631	0.8323	0.6411	0.3589	0.3130	0.2380
Gas locked	0.4984	1.0730	0.7128	0.8443	0.1557	0.4791	0.1563
Standing valve leakage	1.0114	1.0538	0.9729	0.5535	0.4465	0.0321	0.2867
Parting rod	0.6423	0.9795	0.8750	0.7289	0.2711	0.2400	0.1023

TABLE II
CONFUSION MATRIX BASED ON WINDOW SIZE 40 (α =0.3)

Predicted working state	*Collected working state*					
	Normal	Insufficient liquid supply	Gas affected	Gas locked	Standing valve leakage	Parting rod
Normal	36	0	4	0	0	0
Insufficient liquid supply	0	36	4	0	0	0
Gas affected	3	2	35	0	0	0
Gas locked	0	0	0	40	0	0
Standing valve leakage	3	0	0	0	37	0
Parting rod	0	0	0	0	0	40

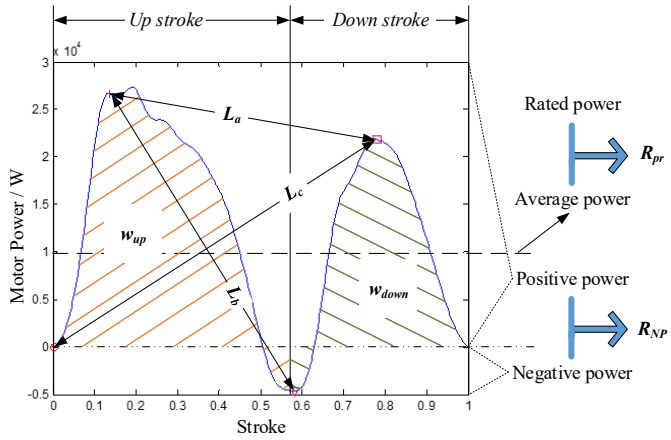

Fig. 10. The seven features on the motor power curve.

with four different colors for their corresponding working point potential region.

Fig. 8 and Fig. 9 illustrate the calculation of valve's working points. In Fig. 8, the blue line stands for the curvature of a motor power curve in one stroke. Based on the proposed average power segmentation method, the four maximum curvature change points are marked in red. And there are four black points obtained by considering the curvature change. These points are again colored, and one can see that red points are more scattered than black points. Moreover, in Fig. 9, these points are translated back on the motor power curve. The proposed approach gives four points at the peaks and valleys of this curve, as discussed in Section II. If instead, we only consider curvature, several calculated valve working points will appear at wrong positions; for example, see the two closely adjacent black points on the left crest. Fig. 9 shows that the proposed method could locate the valve working points on the actual motor power data accurately.

2) *The proposed seven features*

In Fig. 10, seven features are extracted from the motor power curve based on the valve's working points and the average power. The features L_a, L_b, and L_c are the distances between the valve's working points. The red-shaded region corresponds to the up-stroke movement of the rod and the blue-shaded region corresponds to the down-stroke movement. The rations of work done by these two regions to the work done in the whole stroke denote w_{up} the w_{down} respectively. As for the two power ration features on the right side, the R_{NP} is obtained by calculating the positive power and the negative power of this curve by the Eq. (11) and the R_{pr} can be determined using the Eq. (12) based on the average power and the rated power of the motor. The experimental result verifies that all the proposed seven features have obvious physical meaning and they can be applied on a variety of power curves generated by different SRP working states.

The average values of the seven features of the training set are given in Table I. One can see that each working state has

some distinctive characteristics. For example, the *Normal* has the biggest R_{pr}, larger L_a, and the smallest R_{NP}, the *Insufficient Liquid Supply* embodies the highest value of L_c, the *Gas affected* gives the larger L_b, w_{np}, and R_{NP} simultaneously, and so does the *Gas locked*, *Standing valve leakage* and *Parting rod* show their distinctive characters on these features respectively. These experimental results show the independence at each working state that could offer a useful observation sequence for modeling and diagnosing.

C. Working state diagnosis and discussion

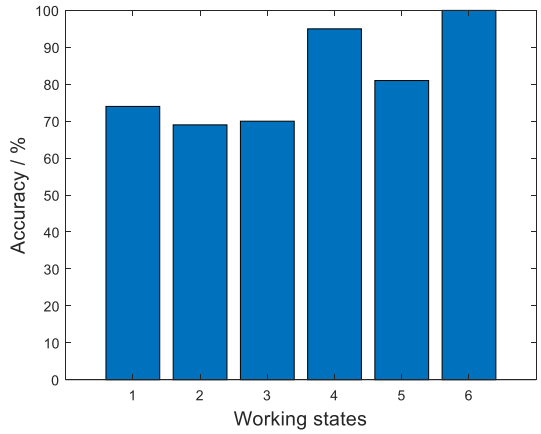

Fig. 11. Diagnosis results of standard HCRF

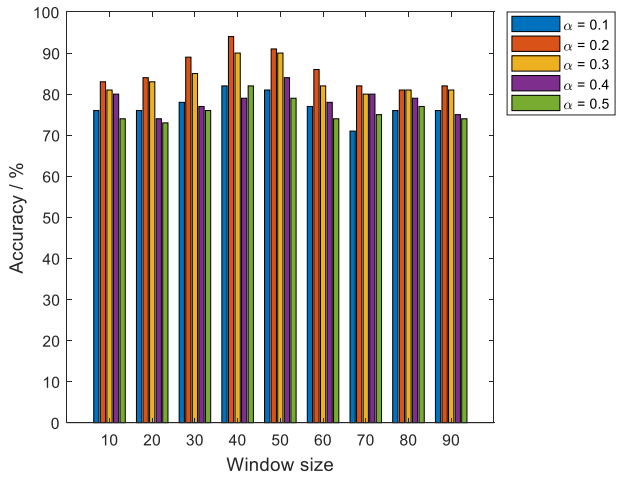

Fig. 12. Comparison of using different window sizes

Two experiments, with and without sampling windows, are conducted to show the diagnosis results. They are depicted by two bar charts in Fig. 11 and Fig. 12.

In this case, an accuracy function that calculates the difference between prediction and actual classification is used for measuring the diagnosis accuracy. It is formulated as follows:

$$Accuracy = \frac{\sum_{i=1}^{T} assess(t_i)}{|T|} \tag{24}$$

$$assess(t_i) = \begin{cases} 1 & if\ classify(t_i) = S_j \\ 0 & otherwise \end{cases} \tag{25}$$

where T is the number of the testing samples, t_i is the i^{th} testing sample, and S_j is the j^{th} working state.

Under the framework illustrated in Fig. 5, the data collected by the NEU device are used to train and identify SRP working states. Without considering the sampling time window, the performance of MHCRFs is shown in Fig. 11. Here, six bars marked 1 to 6 stand for the diagnosing accuracy of working states *Normal*, *Insufficient Liquid Supply*, *Gas affected*, *Gas locked*, *Standing valve leakage* and *Parting rod*, respectively. These accuracies range from 70% to 100%; some faulty states cannot be accurately identified.

Fig. 12 shows the results from the MHCRFs with the sampling time window. The width of window varies from 10 to 90, and the different weights α (as proposed in Eq. (19)) is used to adjust the affected degree from the samples in the window. In general, the accuracy starts to increase from the window width of 10 to 40, and after that, the accuracy starts to decline. At the window width of 40, the highest accuracy is given far more than 90% under $\alpha = 0.3$.

A confusion matrix is employed to demonstrate the classification results in Table II. In this table, at the working states of *Parting rod* and *Gas locked*, all the 80 samples are correctly identified using the proposed method; however, some samples of other working states are wrongly classified. Four *Normal* samples are misclassified as *Gas affected*, four *Insufficient liquid supply* samples are misclassified as *Gas affected*, three *Standing valve leakage* samples are misclassified as *Normal*, and five *Gas affected* are respectively misclassified as *Normal* and *Insufficient liquid supply*. Among the six considered working states, *Gas locked* and *Parting rod* belong to the severe faults in the application, which can lead to the wells' shut-down if further damages on the mechanical and electric components occur. At these two states, the proposed method gives a completely right diagnosis for all test samples. Regarding other states, there are some ambiguous boundaries between *Normal* and *Stand valve leakage*, or *Gas affected* and *Insufficient liquid supply*. For example, when the working state transitions from *Normal* to *Insufficient liquid supply*, there is an overlap area between these two states, which may cause misclassification. At this situation, even experienced engineers are hard to give exact conclusions on the distinction between these working states. On the perspective of practice, these four states belong to the secondary faults and we notice that these minor faults commonly appear in SRP operation, but they will not damage the equipment immediately; instead, they need to be monitored closely for defect progression. Hence, the experimental result is feasible for the application of the SRP diagnosis.

D. Compared with other methods and discussion

To compare the proposed MHCRFs with other several classical methods, three data-driven models – Extreme Learning Machine (ELM), Support Vector Machine (SVM) and Hidden Markov Model (HMM) – are applied on the same data. These alternative models are useful tools for fault diagnosis problems and often appear in literature [7], [4], and [9]. As the motor power data are time series signals, in this study, the conventional feature analysis methods, FFT and

Wavelet transformation, are employed for a comparison study with the proposed features.

TABLE. III
THE COMPARISON OF DIAGNOSIS RESULTS WITH SOME CONVENTIONAL METHODS

Feature extraction methods	*Modeling methods*			
	ELM	SVM	HMM	MHCRFs
FFT	63.75%	66.25%	74.58%	80.42%
Wavelet	65.00%	70.80%	73.33%	82.08%
Proposed features	72.91%	78.57%	81.25%	93.33%

The comparison of diagnosis results from different methods is presented in Table III. In this table, there are totally 12 methods (3 feature extract methods times 4 classification models) applied on the same data. The ELM model gives the lowest accuracy compared to other three models, especially it has only 63.75% accuracy if features are extracted from FFT. As for the SVM model, it shows a higher accuracy when using the Wavelet feature extraction than using the FFT, but it is still lower than using the proposed features. The HMM model has a better performance than ELM and SVM, but it is still worse than the proposed MHCRFs, which gives 93.33% accuracy. Moreover, the table shows that a model based on the proposed features consistently beats the models with Wavelet or FFT-based features.

To give a fair comparison, in the following study, the three conventional models, ELM, SVM, and HMM, are used as binary classifiers and they are embedded into the proposed framework in Eq. 14 to Eq. 16. For convenience, they are renamed as MELMs, MSVMs, and MHMMs. Their diagnosis results with different feature extraction methods are given in Table IV.

TABLE IV
THE COMPARISON OF DIAGNOSIS RESULTS WITH SOME CONVENTIONAL METHODS UNDER THE PROPOSED FRAMEWORK.

Feature extraction methods	*Modeling methods*			
	MELMs	MSVMs	MHMMs	MHCRFs
FFT	66.25%	71.25%	78.75%	80.42%
Wavelet	67.92%	71.25%	79.16%	82.08%
Proposed features	74.12%	81.25%	87.08%	93.33%

From the results shown in Table IV one can see that, under the proposed framework, MELMs and MSVMs have slightly higher diagnostic accuracy than the standard ELM and SVM based on any type of feature set. The FFT-based MELMs presents the lowest accuracy, which is 66.25% that has a 2.5% increase compared with FFT-based ELM in Table III. As for the MHMMs, it gives larger improvements on all three types of features, which are 4.17%, 5.83%, and 5.83%, respectively. Notably, this table clearly shows that, by using the proposed features, all models obtain a higher accuracy than based on the FFT or Wavelet features. However, the MHCRFs with proposed features has the highest accuracy, as shown in the table, because the proposed feature extraction method has the following advantages: First, unlike FFT or Wavelet features, the proposed features consider the mechanism of SRP, which could give mutually independent feature vectors under different working states, as discussed in Table I. Second, the proposed method fully considers the distribution of collected data and gives an appropriate framework for modeling these distributions. Moreover, as the oil exploitation using SRP is a time-varying process, the designed time window provides the flexibility to the model on fitting the varying trend. In addition, the HCRFs has an advantage in dealing with the time series signal, because its diagnosis result is made upon considering all the observations, instead of only considering the current observation like HMM.

V. CONCLUSION

As a replacement to the dynamometer card-based online SRP diagnosis method [4-9], this paper has proposed a new method to diagnose SRP working states using motor power data. This proposed method utilizes mechanism analysis to extract features from data by locating the key working points on the motor power curve. These features are able to characterize the properties of motor power data at valve working points and summarize the power distribution in one stroke. Moreover, considering the motor power data is a time series signal, the HCRFs are used as classifiers under the specific framework that has fully considered the distribution of collected data. In addition, the time window is added into the HCRFs' features function to adapt the work-point drifting of SRP. Furthermore, in order to provide data support for experiments, a self-developed instrument is deployed in the oil field for a long period. Finally, we conducted experiments using the field data and made a comparison of multiple models and feature extraction methods. The result shows that the proposed method is able to achieve a higher accuracy for the SRP working state diagnosis.

REFERENCES

[1] B. M. Wilamowski, O. Kaynak, "Oil well diagnosis by sensing terminal characteristics of the induction motor," *IEEE Transactions on Industrial Electronics,* vol. 47, pp. 1100-1107, Oct. 2000.

[2] J. F. Keating, R. E. Laine, J.W. Jennings, "Application of a Pattern-Matching Expert System to Sucker-Rod, Dynamometer-Card Pattern Recognition," *SPE Production Operations Symposium*, *Oklahoma City*, *Oklahoma*, DOI: https://doi.org/10.2118/21666-MS, pp. 323-333, Apr. 1991.

[3] H. J. Derek, J. W. Jennings, and S. M. Morgan, "Sucker rod pumping unit diagnostics using an expert system," *Permian Basin Oil and Gas Recovery Conference*, *Midland*, *Texas*, DOI: https://doi.org/10.2118/17318-MS, pp, 391-398, March 1988.

[4] K. Li, X. Gao, Z. Tian, et al., "Using the curve moment and the PSO-SVM method to diagnose downhole conditions of a sucker rod pumping unit," *Petroleum Science*, vol. 10, pp. 73-80, Mar. 2013.

[5] G. Han, C. Tan, Jun Li, et al., "Determination of Oil Well Production Rate by Analysis of the Real-Time Dynamometer Card," *SPE Annual Technical Conference and Exhibition*, *Dubai*, *UAE*, DOI: https://doi.org/10.2118/181534-MS, pp 1-22, Sep. 2016.

[6] P. Xu, S. Xu, H. Yin, "Application of self-organizing competitive neural network in fault diagnosis of sucker rod pumping system," *Journal of Petroleum Science and Engineering*, vol. 58, pp. 43-48, Aug. 2007

[7] K. Li, Y. Han, T. Wang, "A novel prediction method for down-hole working conditions of the beam pumping unit based on 8-directions chain codes and online sequential extreme learning machine," *Journal of Petroleum Science and Engineering*, vol. 160, pp. 285-301, Jan. 2018.

[8] A. Zhang, X. Gao, "Supervised dictionary-based transfer subspace learning and applications for fault diagnosis of sucker rod pumping systems," Neurocomputing, vol. 338, pp. 293-306, Feb. 2019.

[9] B. Zheng, X. Gao, "Sucker rod pumping diagnosis using valve working position and parameter optimal continuous hidden Markov model," *Journal of Process Control*, vol. 59, pp. 1-12, Nov. 2017.

[10] S. K. Yadav, K. Tyagi, B. Shah, et al., "Audio signature-based condition monitoring of internal combustion engine using FFT and correlation approach," *IEEE Transactions on Instrumentation and Measurement*, vol. 59, Vol. 60, pp 1217-1226, April 2011.

[11] J. M. Gillis, W. G. Morsi, "Non-intrusive load monitoring using semi-supervised machine learning and Wavelet design," *IEEE Transactions on smart grid*, vol. 8, pp. 2648-2655, Nov. 2017.

[12] X. Jiang, F. Wu, Y. Zhang, et al., "The classification of multi-modal data with Hidden Conditional Random Field," *Pattern Recognition Letters*, vol. 51, pp. 63-69, Jan. 2015.

[13] S. P. Chatzis, D. I. Kosmopoulos, P. Dolitis, "A conditional random field-based model for joint sequence segmentation and classification," *Pattern Recognition*, vol. 46, pp. 1569-1578, Jun. 2013.

[14] W. Wen, R. Cai, Z. Hao, et al., "Recognizing activities from partially observation stream using posterior regularized conditional random fields," *Neurocomputing*, vol. 260, pp. 294-301, Oct. 2017.

[15] A. Liu, W. Nie, Y. Su, et al., "Coupled Hidden conditional random fields for RGB-D human action recognition. *Signal Processing*, vol. 112, pp. 74-82, July 2015.

[16] L. Liu, Y. Cheng, S. Zhang, "Conditional random field reliability analysis of a cohesion-frictional slope," *Computers and Geotechnics*, vol. 82, pp. 173-186, Feb. 2017.

[17] L. Albert, F. Rottensteiner, C. Heipke, "A higher order conditional random field model for simultaneous classification of land cover and land use," *ISPRS Journal of Photogrammetry and Remote Sensing*, vol. 130, pp. 63-80, Aug. 2017.

[18] S. Kosov, K. Shirahama, C. Li, et al., "Environmental microorganism classification using conditional random fields and deep convolutional neural networks," *Pattern Recognition*, vol. 77, pp. 248-261, May. 2018.

[19] A. Quattoni, S. Wang, L. Morency, et al., "Hidden Conditional Random Fields," *IEEE Transactions on Pattern Analysis and Machine Intelligence*, Vol. 29, pp. 1848-1853, Oct. 2007.

[20] M. H. Siddiqi, R. Ali, A. M. Khan, et al., "Human facial expression recognition using Stepwise Linear Discriminant Analysis and Hidden Conditional Random Fields," *IEEE Transactions on Image Processing*, Vol. 24, pp. 1386-1398, April 2015.

[21] M. Fang, H. Kodamana, B. Huang, et al., "A novel approach to process operating mode diagnosis using conditional random fields in the presence of missing data," *Computers and Chemical Engineering*, Vol. 111, pp. 149-163, Mar. 2018.

[22] K. Bousmalis, S. Zafeiriou, L. Morency, et al., "Variational infinite Hidden Conditional Random Fields," *IEEE Transactions on Pattern Analysis and Machine Intelligence*, Vol. 37, pp. 1917-1929, Sep. 2015.

[23] P. Tang, T. W. S. Chow, "Wireless sensor-networks conditions monitoring and fault diagnosis using neighborhood Hidden Conditional Random Field," *IEEE Transactions on Industrial informatics*, Vol. 12, pp. 393-940, June 2016.

Boyuan Zheng received the B.S. and M.S. degrees in control theory and control engineering from Liaoning University of Petroleum and Chemical Technology, Fushun, China, in 2012 and 2015. He is currently working toward the Ph.D. degree in control theory and control engineering in the School of Information Science and Engineering at Northeastern University, Shenyang, China.

His research interests include diagnosis, soft sensor, prognostics and health management, and modeling of complex industry process.

Xianwen Gao received the B.S. degree in automation from Shenyang University of Chemical Technology, Shenyang, in 1978, and the M.S. and Ph.D. degrees in control theory and control engineering from Northeastern University, Shenyang, China, in 1993 and 1998, respectively.

He is currently a Professor at Northeastern University. His research interests include modeling of complex industry process and intelligent control, sliding-mode control, and stochastic jump systems.

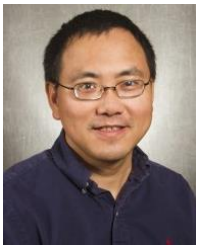

Rong Pan received B.S. Materials Science and Engineering from Shanghai Jiao Tong University, Shanghai, China, in 1995. He received M.S. Industrial Engineering from Florida A&M University in 1999 and his Ph.D. degree industrial engineering from the Pennsylvania State University in 2002.

He is currently an Associate Professor in the School of Computing, Informatics, and Decision Systems Engineering at Arizona State University. His research interests include quality and reliability engineering, design of experiments, time series analysis, and statistical learning theory. He is a senior member of ASQ and IIE, and a member of SRE.